Reversed Peaks of Saturated Absorption Spectra of Atomic Rubidium

Sangkyung Lee[1], Kanghee Lee[1], and Jaewook Ahn[1,2*]

[1]*Department of Physics, KAIST, Daejeon 305-701, Korea*
[2]*Institute of Optical Science and Technology, KAIST, Daejeon 305-701, Korea*

Received July 14, 2008; accepted December 14, 2008; published online March 23, 2009

We have studied the effects of optical pumping and near-resonant radiation pressure that compete with the saturation effect on the formation of the line shapes of Doppler-free saturation absorption spectra of alkali atoms. We have measured the reverse of the sign of $F_g = 3$ to $F_e = 4$ saturated absorption of the rubidium D_2 line and the change in its asymmetry as the optical pumping effect is gradually turned on compared with the saturation effect. The experimentally observed behaviors of optically pumped Lamb dips and crossover resonances in rubidium show good agreement with the calculation using the phenomenological model previously introduced for cesium.

DOI: 10.1143/JJAP.48.032301

1. Introduction

Saturation laser spectroscopy is used to obtain Doppler-free spectra of atomic systems by measuring the absorption of the probe beam that passes through a Doppler-broadened medium of gaseous atoms, which is saturated by a counter-propagating pump beam.[1)] The intense pump beam induces depletion of a velocity-selective portion of the ground-state population of the atomic gas and the depletion becomes a reason for a narrow dip, known as Lamb dip, in the Doppler-broadened absorption curve of the probe beam.[2)] Saturation absorption spectroscopy has been widely used to probe closely spaced fine and hyperfine structures of atoms and molecules with a resolution higher than the ones limited by the Doppler width of transitions. The line profile of the dip, which is a simple Lorentzian in a two-level atomic model, becomes complicated in a closely spaced multilevel system, particularly when the energy difference between the transitions is smaller than the corresponding Doppler width. In principle, a density-matrix formalism for the interaction between multilevel atoms and multiple laser fields can be used to obtain these line profiles of absorption spectra. However, if the experiments are carried out with an ignorable optical coherence between the states, or in other words, at the limit of low pump power, at which the atomic coherence is destroyed by spontaneous emission and atomic collision, the heavy calculational burden of the density matrix formalism can be lifted off by a simpler calculation of rate equations.[3)]

The effect of optical pumping in the saturation optical spectroscopy was first studied by Pappas *et al.*[4)] When a probe beam scans near an optically pumped transition, or a transition from a ground sublevel into which the excited-state population of the pump is decayed, the line profile of the Lamb dip makes a sign change to become a peak.[4)] Theoretical studies of the details of the absorption line shapes of more than two closely lying energy levels in systems are carried out for three-level atoms[5)] and four-level atoms.[6,7)] The change in the saturated spectra of cesium D_2 lines was measured with the change in the pump beam intensity, and the results were explained with a phenomenological model.[8)] Using the model, we attempted to explain the combined effects of the saturation, the velocity-selective optical pumping, and the resonant light pressure.

Recently, Im *et al.*[9)] developed a phenomenological theory to explain the sign reversal of the transition from $F_g = 4$ to $F_e = 5$ of the cesium D_2 line, which appears as the pump beam intensity increases. Moon *et al.*[10)] obtained analytic solutions for saturated absorption spectra of ^{87}Rb by solving a model rate equation and showed that saturated absorption spectra could be well described on the basis of an analytic theory in certain polarization configurations. In this paper, we have further applied these theories to study the change in the shapes of rubidium D_2 lines. The rubidium D_2 lines have been studied for their importance in laser cooling[11)] and Bose–Einstein condensation,[12)] also as a reference signal for the frequency stabilization of laser sources.[13)] We compare experimentally measured spectra of $F_g = 3 \rightarrow F_e$ transitions with the results numerically obtained from our model calculation. Also, we investigate the change in line shapes as a function of the laser intensity and polarizations of the pump and probe beams.

2. Experimental Procedure

The experimental setup was prepared similarly as the standard configuration for the saturated absorption spectroscopy.[14)] The light source is a grating-feedback diode laser with a linewidth of 2–3 MHz and the wavelength of the laser is 780.2 nm tuned for the Rb D_2 line. The Rb D_2 line consists of $5S_{1/2}$ and $5P_{3/2}$ levels. The ground level $5S_{1/2}$ is split into two levels and the first excited level $5P_{3/2}$ is split into four hyperfine sublevels. As shown in Fig. 1, the laser beam is first split into two beams using a beam splitter, one for the pump and the other for the absorption measurement. The second beam is split again using a thick (10 mm) beam splitter into two beams, used for the probe and reference. Both beams are then reflected at the front and back surfaces of the thick beam splitter and pass through a Rb gas cell (length of 100 mm). The vapor pressure of the gas cell was low enough, in the order of 10^{-7} Torr, that the atomic collision can be ignored. The earth magnetic field strength is approximately 50 μT around the vapor cell. The pump beam counterpropagates and overlaps with the probe beam inside the Rb gas cell. The gas cell is maintained at room temperature and the radius of the pump beam is 2 mm. The intensity difference between the probe and reference beams is measured for the elimination of the undesirable Doppler background signal, and the saturated absorption spectra are obtained. The Doppler-free signals are measured as functions of the intensity and polarization angles of the pump and probe beams.

*E-mail address: jwahn@kaist.ac.kr

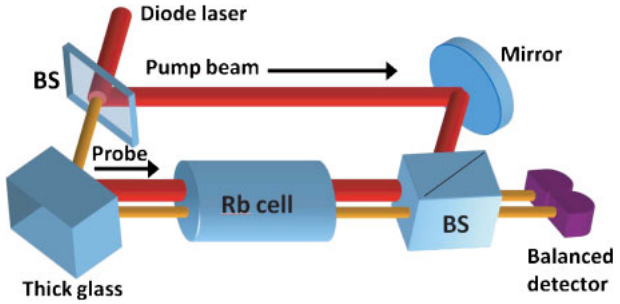

Fig. 1. (Color online) Experiment setup.

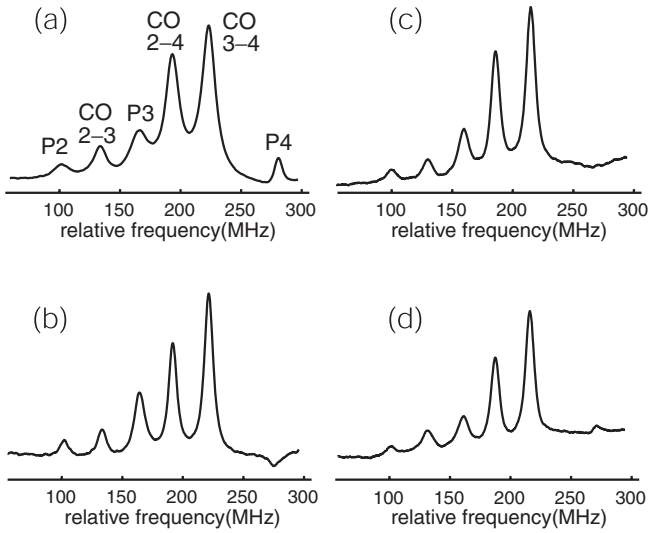

Fig. 2. Saturation absorption spectra of atomic rubidium D_2 lines, showing the three principal resonant transitions $F_g = 3 \rightarrow F_e = 2, 3, 4$, (labeled as P2, P3, and P4) and the crossover transitions (labeled as CO2-3, CO2-4, and CO3-4). The polarizations of the pump and probe beams are both linear. The polarization angle between the linearly polarized pump and the probe beams is denoted as θ. The polarization angle, θ, and the pump beam intensities are (a) $\theta = 0°$ and 8.5 μW/mm^2; (b) $\theta = 0°$ and 1.0 μW/mm^2; (c) $\theta = 0°$ and 0.78 μW/mm^2; and (d) $\theta = 90°$ and 0.78 μW/mm^2.

The ^{85}Rb D_2 line is comprised of the transitions from two ground states ($F_g = 2, 3$) to four excited states ($F_e = 1, 2, 3, 4$). The transitions from $F_g = 2$ and also from $F_g = 3$ have, due to the selection rules, three principal resonances and three crossover resonances. Typical measurements of the saturation absorption line shapes of the transitions from $F_g = 3$ to $F_e = 2, 3, 4$ are shown in Fig. 2. Figures 2(a) and 2(b) show that the line shape of the $F_g = 3 \rightarrow F_e = 4$ transition changes its sign from positive to negative as the pump-beam intensity decreases. If the pump intensity decreases further, the absorption peak disappears as shown in Fig. 2(c). This result of saturation absorption spectra is from a parallel polarization configuration of the pump and probe beams. For the orthogonal polarization configuration, on the other hand, the peak reversal does not appear, and the peak of the $F_g = 3 \rightarrow F_e = 4$ transition still remains positive for the very low pump intensity, as in Fig. 2(d).

3. Optical Pumping in Two- and Four-Level Atoms

The behaviors of the three transitions $F_g = 3 \rightarrow F_e = 2, 3, 4$ as functions of the pump-beam intensity are shown in Fig. 3.

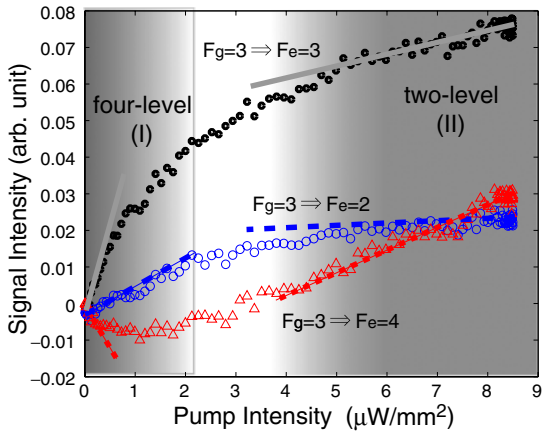

Fig. 3. (Color online) Probe transmissions of rubidium D_2 lines: The behaviors of the signal changes of $F_g = 3 \rightarrow F_e = 2, 3, 4$ resonance peaks are shown as functions of the pump intensity. As the pumping power increases, the four-, three-, and two-level models become sequentially adequate to explain the signal behavior. The results of the four- and two-level model calculations are shown as the solid lines for $F_g = 3 \rightarrow F_e = 3$, as the long dotted lines for $F_g = 3 \rightarrow F_e = 2$, and as the short dotted lines for $F_g = 3 \rightarrow F_e = 4$.

We first analyze those behaviors of line-shape changes in terms of the saturation and optical-pumping effects modeled in pseudo two- and four-level atomic systems in this section; the additional asymmetric behavior of $F_g = 3 \rightarrow F_e = 4$ transition will be addressed in the following section.

In particular, $F_g = 3 \rightarrow F_e = 4$ transition shows a sign reversal in the low-pump-intensity regime (I) as in Fig. 3. In the low-pump-intensity regime, the pump field accumulates atomic population to the inner Zeeman sublevels, relatively increasing the probe absorptions (only $\Delta m_F = 0$ transitions), and, as a result, $F_g = 3 \rightarrow F_e = 4$ transition shows a sign change. Therefore, the transmissive probe signal decreases as the atomic population is further redistributed using a stronger pump beam, only in the low-pump-intensity regime. When the pump intensity further increases, the allowed transitions become saturated and the probe signal then gradually increases, similar to the behavior of saturated optical spectra of a two-level system. In other words, as measured in Fig. 3, below a certain intensity limit (~2 μW/mm^2 in rubidium for $F_g = 3 \rightarrow F_e = 4$), the spontaneous emission rate Γ_{sp} of this transition is larger than the absorption rate ($\sigma I/\hbar\omega \ll \Gamma_{sp}$), where σ and I denote the absorption cross section and the laser intensity, respectively.

On the other hand, in the other transitions, the populations of the outer Zeeman sublevels, for example, $m_F = \pm 3$ in the $F_g = 3 \rightarrow F_e = 2$ transition, increase via the optical pumping so the transmissive probe signal increases as the pump intensity increases. In these later cases, the linearly polarized probe beams cannot probe the outermost Zeeman sublevels; for example, $m_F = \pm 3$ in the $F_g = 3 \rightarrow F_e = 2$ transition, the positive dip arises in the transmissive probe signal. As a result, in these transitions, the probe signals never decrease and continue increasing as the pump intensity increases.

Conceptually, we can estimate the relative magnitudes of the resonances by considering all the transition probabilities. As the transition probabilities in Fig. 4 indicate, the diagonal transitions toward $m_F = 0$ are dominantly stronger in $F_g = 3 \rightarrow F_e = 4$ and also in $F_g = 2 \rightarrow F_e = 3$ transitions than

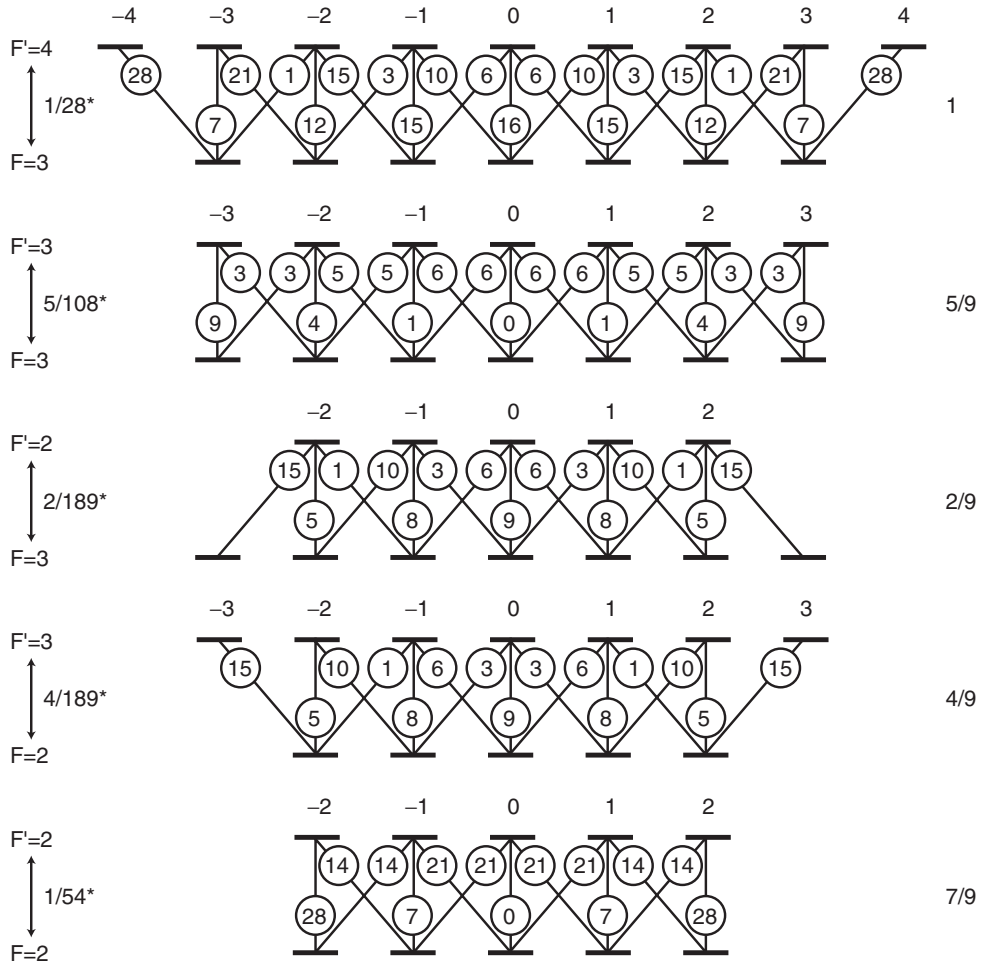

Fig. 4. Normalized transition probabilities between all magnetic sublevels in the rubidium D_2 resonance line. The factors on the right give the total statistical weight of the transition between levels F_g and F_e. For example, the $F_e = 4$ level decays only to the $F_e = 3$ level, whereas the $F_e = 3$ level decays into the $F_g = 3$ level with a total probability of 5/9 and into the $F_g = 2$ level with a total probability of 4/9. The numbers in the circles have to be multiplied by the factor on the right-hand side of the diagram.

the transitions toward higher m_F sublevels, causing the increase in the probe transition level. On the other hand, in $F_g = 3 \rightarrow F_e = 2$, the diagonal transitions toward higher $|m_F|$ sublevels are stronger than the ones toward lower $|m_F|$'s, and, therefore, the probe signal should decrease. In the $F_g = 3 \rightarrow F_e = 3$ and $F_g = 2 \rightarrow F_e = 2$ transitions, the innermost $m_F = 0$ sublevels will gather populations but, in this case, the transition rate of $\Delta m_F = 0$ excitation is zero, so the overall probe transition should decrease. To further simplify the calculation, we can assume that the atomic population in the ground state is dominantly bigger than that in the excited states. We note that the equilibrium population, defined as the ratio between the populations in the excited state and ground state is $N_e/N_g \approx 4.42 \times 10^{-5}$ at room temperature.

In the following paragraph, we use Nakayama's model[6] to quantitatively describe the above scenario. In Nakayama's four-level model, the N-level atomic system is divided into a set of two-level, three-level, and four-level subsystems. The main prediction of Nakayama's theory was the confirmation of the existence of the negative dip in the regime of low pump intensity.

$F_g = 3 \rightarrow F_e = 4$ transition consists of 7 two-level systems and 12 four-level systems. There are no three-level systems because of the selection rule. In a $\theta = 0^\circ$ configuration, or when the pump and probe polarizations are parallel with each other, the selection rule $\Delta m_F = 0$ is applied and, as a result, only two-level and four-level systems are allowed, but not the three-level systems. As seen before, if the spontaneous decay into the original ground state is dominantly bigger than decays into other ground states, we can then treat the N-level energy system like a two-level system, as in Fig. 5(a). In this case, the transmission of the probe becomes a positive dip. On the other hand, if the spontaneous decay into other ground states, compared with the original ground state, is not negligible, a four-level system can be used to describe the static condition of atomic population. As shown in Fig. 5(b), the spontaneous decay, marked as a dotted line in the figure, makes nonzero ground-state population, only when the pump beam exists, and as a result, the measured differential transmission signal of the probe becomes negative. Similarly, in the $\theta = 90^\circ$ polarization configuration, two three-level and one three-level systems need to be considered and they are shown in Figs. 5(c)–5(e). A positive dip of the probe transmission, in this $\theta = 90^\circ$ case, appears from the system (c) in Fig. 5, because of a similar reason as for the system (a) in the $\theta = 0^\circ$ case. We may say that the system (c) in the $\theta = 90^\circ$ polarization case is equivalent to the system (a) in the $\theta = 0^\circ$ case because in both systems (a) and (c), the

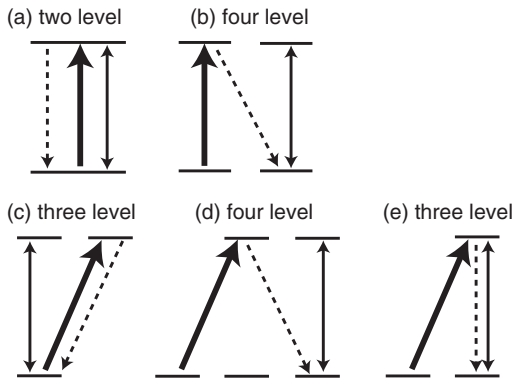

Fig. 5. Level system for $F_g = 3 \rightarrow F_e = 2, 3, 4$ considering Zeeman sublevels; each transition contains two-level and four-level systems. The polarization angles, θ, between the pump and probe for each configuration are: $\theta = 0°$ for (a) and (b), and $\theta = 90°$ for (c), (d), and (e). The transitions in (a) and (c) make positive dips but the transitions in (b), (d), and (e) induce negative dips.

pump and probe are both resonant to the particular two-level system, and, as a result, both show positive dips. The level systems (d) and (e) make a negative dip in the probe transmission for a similar reason as in the case of the system (b). After all, an overall shape, including the sign, of the transmission signal is determined as a sum of all possible transitions in those systems.

We now calculate the principal resonance shapes of saturation absorption spectroscopy of ^{85}Rb. First, the optical pumping effect contributes to a principal resonance as

$$L^i_{jj,k:\mathrm{OP}} = N_g I_{ij,k} S_k \frac{(\Delta\nu/2)^2}{(\nu - \nu_k)^2 + (\Delta\nu/2)^2}, \qquad (1)$$

where N_g, $\Delta\nu$, and ν_k denote the ground-state population, the saturation linewidth, and the frequency of the kth principal resonance, respectively. The relative magnitude of a particular four-level system is $I_{ij,k} = |\mu_i|^2|\mu_j|^2(-\delta_{i,\mathrm{sp}} + |\mu_{\mathrm{sp}}|^2/\Gamma_F)$, where $|\mu_i|^2$, $|\mu_j|^2$, and μ_{sp} are the probabilities of transitions corresponding to the pump beam, the probe beam, and the spontaneous emission from the excited state, respectively. Kronecker's delta function $\delta_{i,\mathrm{sp}}$ denotes the depopulation of the ground state by the pump beam, and Γ_F is the total transition probability of the Zeeman sublevel. The saturation factor S_k is related to the intensity of the kth resonance as follows:

$$S_k = \frac{I_p/I_{\mathrm{eff},k}}{(1 + I_p/I_{\mathrm{eff},k})^{1/2}[1 + (1 + I_p/I_{\mathrm{eff},k})^{1/2}]}, \qquad (2)$$

where I_p is the pump beam intensity. The effective saturation intensity is $I_{\mathrm{eff},k} = (\tau_e/\tau_{\mathrm{eff}})I_{\mathrm{sat}}$. The saturation intensity $I_{\mathrm{sat}} = 16\,\mu\mathrm{W/mm}^2$ is numerically estimated. The effective atomic lifetime τ_{eff} is given by $\tau_{\mathrm{eff}} = \tau_g + \tau_e - \Gamma_{eg}\tau_e\tau_g$, where Γ_{eg} is the rate of the partial transition from the excited state to the ground state and τ_e (τ_g) is the excited (ground)-state lifetime. As atomic collisions can be neglected, the ground-state lifetime is the same as the transit time of an atom crossing a transverse beam diameter and $\tau_g = 13.6\,\mu\mathrm{s}$ is estimated. The excited state lifetime τ_e of $5P_{3/2}$ is 25.5 ns.

In the configuration of $\theta = 0°$, the total $I_{ij,k}$ is the sum of all the two- and four-level systems of all Zeeman sublevels. As listed in Table I, $I_{ij,k}$'s are calculated as $I_{ij,k} = 0.0240$ for $F_g = 3 \rightarrow F_e = 2$, $I_{ij,k} = 0.212$ for $F_g = 3 \rightarrow F_e = 3$, and $I_{ij,k} = -0.103$ for $F_g = 3 \rightarrow F_e = 4$. In our differential measurement, the positive (negative) I represents a positive (negative) probe transmission. In eq. (1), the principal resonance is proportional to $I_{ij,k}$, relative magnitude for the involved model system, and S_k, the saturation factor. The saturation factor is approximately linear in the weak-pump-intensity regime, so $I_{ij,k}$ mainly contributes to the deviating tendency from a linear behavior of the transmission signal. Therefore, we can use the initial slopes of the probe transmission peaks in Fig. 3 with the calculated $I_{ij,k}$ values, and we found that they are in good agreement. On the other hand, at $\theta = 90°$, $I_{ij,k} = 0.0113$ for $F_g = 3 \rightarrow F_e = 2$, $I_{ij,k} = 0.0541$ for $F_g = 3 \rightarrow F_e = 3$, and $I_{ij,k} = 0.0517$ for $F_g = 3 \rightarrow F_e = 4$. In our experiment, those peaks remain positive in the range of the pump intensity measurement.

Table I. Calculated $I_{ij,k}$'s for the principal resonances of ^{85}Rb D_2 lines.

Transition	$\theta = 0°$	$\theta = 90°$
$F_g = 3 \rightarrow F_e = 2$	0.0240	0.0113
$F_g = 3 \rightarrow F_e = 3$	0.212	0.0541
$F_g = 3 \rightarrow F_e = 4$	−0.103	0.0517

In the high-pump-intensity regime (II), the effect of stimulated emission becomes a lot bigger than that of spontaneous emission. As a result, the system becomes a pseudo two-level system, or the effects due to the presence of Zeeman sublevels become significantly reduced. In an optically saturated pseudo two-level system, the transition probability is obtained considering only the saturation effect using the pump beam. Therefore, the line shape in the regime of high field becomes

$$L^i_{jj,k:\mathrm{SAT}} = N_g|\mu_k|^2 S_k \frac{(\Delta\nu/2)^2}{(\nu - \nu_k)^2 + (\Delta\nu/2)^2}, \qquad (3)$$

where the transition dipole moment $|\mu_k|$ determines the transition probability. We obtain $|\mu_k|^2 = 0.222$ for $F_g = 3 \rightarrow F_e = 2$, $|\mu_k|^2 = 0.556$ for $F_g = 3 \rightarrow F_e = 3$, and $|\mu_k|^2 = 1$ for $F_g = 3 \rightarrow F_e = 4$. We note that the S_k asymptotically approaches 1 in the limit of high pump power, or in the regime of optical pumping in a two-level system (II). The slopes in Fig. 3, as a result, become proportional to μ_k^2's in the high-pump-intensity regime (II).

4. Frequency Shift of Principal Resonance due to Polarization and Light Pressure Effects

In the low-pump-intensity regime, the line shape of the $F_g = 3 \rightarrow F_e = 4$ transition becomes asymmetric, owing to the light pressure effect.[8] The velocity of an atom changes because of the momentum exchange with the incident photon. The momentum exchange causes a small asymmetric modification to the distribution of atomic velocity. The asymmetric velocity distribution results in an asymmetric absorption line shape of Doppler-free spectroscopy. The line shape function pertinent to this light pressure effect is described as

$$L^i_{jj,k:\mathrm{LP}} = 2N_g\epsilon_r\tau_{\mathrm{tr}}S_k(\nu - \nu_k)\frac{(\Delta\nu/2)^3}{[(\nu - \nu_k)^2 + (\Delta\nu/2)^2]^2}, \qquad (4)$$

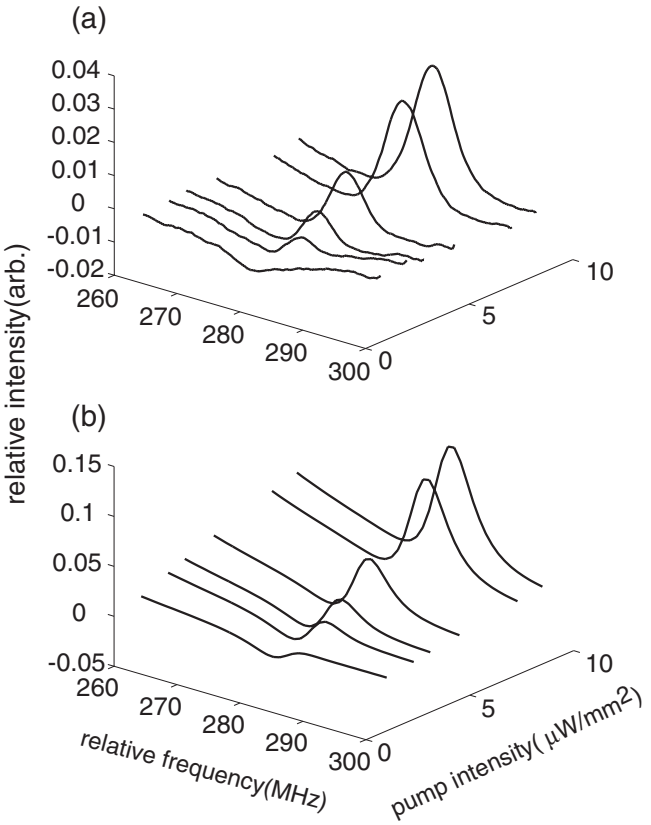

Fig. 6. Spectral line shapes for $F_g = 3 \rightarrow F_e = 4$ transitions at the polarization angle $\theta = 0°$. The experimental measurements in (a) and the numerical simulations in (b) are compared.

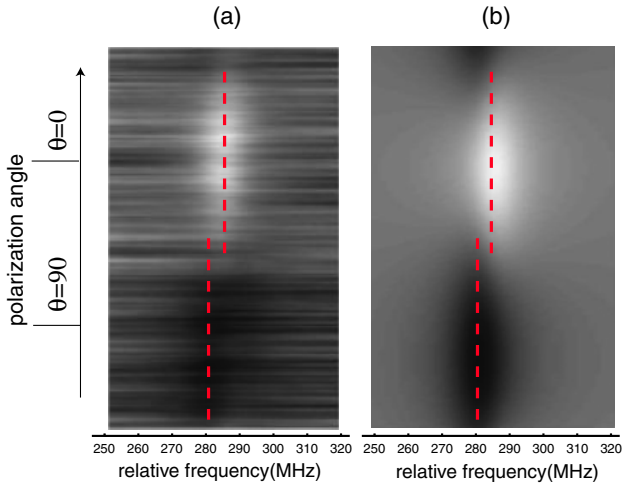

Fig. 7. (Color online) Polarization dependence of $F_g = 3 \rightarrow F_e = 4$ resonance peak: The experimental (a) and the simulation (b) data are drawn in the two-dimensional plane of laser frequency (x-axis) and polarization angle (y-axis). The dotted lines indicates the shift of the center of the absorption dip. The shift is approximately 6 MHz in our experiment.

where ϵ_r is the recoil energy divided by $\hbar$ and τ_{tr} is the transit time. The total line shape in the low-pump-intensity regime, can be described as the sum of the optical pumping term, $L^i_{jj,k:\mathrm{OP}}$, and the light pressure term, $L^i_{jj,k:\mathrm{LP}}$. In general, the latter effect is very small compared with the former, because of the scaling of pump and saturation intensities: $2I_p/I_{sat}\epsilon_r\tau_{tr} \approx 0.04$. However, the net effect of $L^i_{jj,k:\mathrm{OP}}$ and $L^i_{jj,k:\mathrm{LP}}$ on the absorption signal makes an asymmetric line shape. The measured and calculated line shapes are compared well in Fig. 6. In the high-pump-intensity case, as in the last two curves in the figure, the line shapes are mostly determined by saturation effect.

The asymmetric line shape change caused by the light pressure effect can either blue-shift or red-shift the resonance peak position in frequency. The light pressure effect reduces the red detuned part and raises the blue detuned part of the resonance line shape. As a result, if the resonance peak is originally a positive (negative) dip, then the light pressure effect shifts the resonance toward the blue-shift (red-shift) direction.

Also, the sign of the resonance peak is, as we discussed, dependent on the polarization configuration between the pump and probe beams. Particularly, the resonance peak of $F_g = 3 \rightarrow F_e = 4$ shows a negative dip for the $\theta = 0°$ polarization case, as seen in Fig. 2. This same resonance peak becomes a positive one as the polarization angle changes to $\theta = 90°$. In our experiment, we measured the frequency shift of $F_g = 3 \rightarrow F_e = 4$ transition as a function of the polarization angle θ between the pump and probe beams.

We can decompose the polarization dependence of the resonance line shape into two independent terms, parallel and perpendicular. As we designate the linear polarization angle between the pump and probe beam as θ, the magnitude of the signal is proportional to an electric susceptibility.[6] The saturation signals are, therefore, obtained as the imaginary parts of the susceptibilities related to the absorption coefficient as

$$I_\theta \propto \mathrm{Im}[\chi^0_{00} + \chi^{\pm}_{00}] \propto I_\parallel + I_\perp, \tag{5}$$

or proportional to the individual saturation signals, $I_\parallel$ and $I_\perp$, in the parallel and perpendicular polarizations, respectively. Here, χ^0_{00} and $\chi^{\pm}_{00}$ denote the susceptibilities in parallel and perpendicular pump polarization configurations, respectively. As a result, we can include the polarization effect to the previously discussed model calculation and the magnitude of the signal $L_k(I_p, \theta)$ becomes

$$L_k(I_p, \theta) = L_{k,\parallel}[I_p \cos^2(\theta)] + L_{k,\perp}[I_p \sin^2(\theta)], \tag{6}$$

where $L_{k,\parallel}$ ($L_{k,\perp}$) is the magnitude of the kth resonance under the parallel (perpendicular) polarization condition. In Fig. 7, at $\theta = 0°$, we note that the negative dip shifts the resonance dip toward the lower frequency direction. Likewise, at $\theta = 90°$, the location of the resonance shifts to the higher frequency. The net variation of the resonance shift is measured as 6 MHz. This value is in good agreement with the numerical estimation from eq. (4).

5. Summary and Conclusions

In conclusion, we have measured the reverse of the sign of $F_g = 3$ to $F_e = 4$ saturated absorption of the rubidium D_2 line and the change in its asymmetry as the optical pumping effect is gradually turned on compared with the saturation effect. We have obtained the saturated absorption spectra as functions of the intensity and polarization of pump beam. The saturated absorption spectra of the rubidium D_2 line are well described using the phenomenological model, which

considers the optical pumping effect and the light pressure effect. Moreover, the model describes the frequency shift in the low-intensity regime that is caused by the combined effects of light pressure and polarization. The experimentally observed behaviors of optically pumped Lamb dips and crossover resonances in rubidium show good agreement with the phenomenological model calculation.

Acknowledgments

This work was supported by MOHERD Grant KRF-2005-205-C00024 and IT R&D program of MKE/IITA 2008-F-021-01.

1) T. W. Hänsch, M. D. Levenson, and A. K. Schawlow: Phys. Rev. Lett. **26** (1971) 946.
2) W. E. Lamb, Jr.: Phys. Rev. **134** (1964) A1429.
3) H. Rinneberg, T. Huhle, E. Matthias, and A. Timmermann: Z. Phys. A **295** (1980) 17.
4) P. G. Pappas, M. M. Burns, D. D. Hinshelwood, and M. S. Feld: Phys. Rev. A **21** (1980) 1955.
5) H. R. Schlossberg and A. Javan: Phys. Rev. **150** (1966) 267.
6) S. Nakayama: Jpn. J. Appl. Phys. **24** (1985) 1.
7) S. Nakayama: Jpn. J. Appl. Phys. **23** (1984) 879.
8) R. Grimm and J. Mlynek: Appl. Phys. B **49** (1989) 179.
9) K.-B. Im, H.-Y. Jung, C.-H. Oh, S.-H. Song, P.-S. Kim, and H.-S. Lee: Phys. Rev. A **63** (2001) 034501.
10) G. Moon and H.-R. Noh: J. Opt. Soc. Am. B **25** (2008) 701.
11) C. E. Wieman, G. Flowers, and S. Gilbert: Am. J. Phys. **63** (1995) 317.
12) M. H. Anderson, J. R. Ensher, M. R. Mathews, C. E. Wieman, and E. A. Cornell: Science **269** (1995) 198.
13) V. V. Yashchuk, D. Budker, and J. R. Davis: Rev. Sci. Instrum. **71** (2000) 341.
14) K. B. MacAdam, A. Steinbach, and C. Wieman: Am. J. Phys. **60** (1992) 1098.